Research Paper
J. Astron. Space Sci. 38(3), 165-173 (2021)
https://doi.org/10.5140/JASS.2021.38.3.165

JASS Journal of Astronomy and Space Sciences

Evaluation of a Laser Altimeter using the Pseudo-Random Noise Modulation Technique for Apophis Mission

Hyung-Chul Lim[1†], Ki-Pyoung Sung[1], Mansoo Choi[1], Jong Uk Park[1], Chul-Sung Choi[1], Seong-Cheol Bang[1], Young-Jun Choi[1,2], Hong-Kyu Moon[1]

[1]Korea Astronomy and Space Science Institute, Daejeon 34055, Korea
[2]University of Science and Technology, Daejeon 34113, Korea

Apophis is a near-Earth object with a diameter of approximately 340 m, which will come closer to the Earth than a geostationary orbit in 2029, offering a unique opportunity for characterizing the object during the upcoming encounter. Therefore, Korea Astronomy and Space Science Institute has a plan to propose a space mission to explore the Apophis asteroid using scientific instruments such as a laser altimeter. In this study, we evaluate the performance metrics of a laser altimeter using a pseudo-random noise modulation technique for the Apophis mission, in terms of detection probability and ranging accuracy. The closed-form expression of detection probability is provided using the cross correlation between the received pulse trains and pseudo-random binary sequence. And the new ranging accuracy model using Gaussian error propagation is also derived by considering the sampling rate. The operation range is significantly limited by thermal noise rather than background noise, owing to not only the low power laser but also the avalanche photodiode in the analog mode operation. However, it is demonstrated from the numerical simulation that the laser altimeter can achieve the ranging performance required for a proximity operation mode, which employs commercially available components onboard CubeSat-scale satellites for optical communications.

Keywords: Apophis mission, proximity operation, laser altimeter, pseudo-random noise modulation, cross correlation

1. INTRODUCTION

When the near-Earth object of 99942 Apophis was discovered in 2004, it was considered a potentially hazardous asteroid with a 2.7% probability of impacting the Earth in 2029. Follow-up measurements from the ground-based optical telescopes and radars have significantly reduced the impact risk, and ruled out the possibility of impact (Brozović et al. 2018). However, Apophis will come as close as a geocentric distance of 5.6 Earth radii (i.e., inside the altitude of geostationary orbit) on April 13, 2029 (Yu et al. 2014; Thuillot et al. 2015; Brozović et al. 2018). The upcoming encounter is so close that tidal stresses and torques due to the Earth's gravity field may not only cause reshaping or small-scale mass motions, but also change the spin state. This will provide an unparalleled opportunity to study the structural and physical properties of the asteroid (Thuillot et al. 2015). In addition, understanding these properties may also provide vital knowledge, such as thermal radiation acceleration, for planetary defense against the possibility of asteroid impact by improving orbital predictions of potentially hazardous asteroids.

Korea Astronomy and Space Science Institute is in the preparation phase to propose a space mission that will launche a spacecraft in 2027 to explore the Apophis asteroid for scientific research and planetary defense. The spacecraft will have a wet mass of 370 kg, containing several scientific instruments that could provide valuable information to characterize the asteroid (Moon et al. 2020). However, rather than a touchdown or sampling return mission, it will

Received 30 JUN 2021 **Revised** 10 AUG 2021 **Accepted** 12 AUG 2021
†**Corresponding Author**
Tel: +82-42-865-3235, E-mail: hclim@kasi.re.kr
ORCID: https://orcid.org/0000-0001-5266-1335

http://janss.kr pISSN: 2093-5587 eISSN: 2093-1409

conduct a proximity operation (i.e., rendezvous mission) to achieve scientific goals. The essential candidates of the scientific instruments include wide/narrow-angle cameras, a polarimetric camera, and a laser altimeter, and the optional instruments include a multi-band imager, a dust particle detector, a magnetometer and others. A laser altimeter has become an essential instrument for determining the shape, rotational and orbital dynamics, and surface structural and internal properties with gravity measurements for small planetary bodies (Sun et al. 2021). In particular, it not only plays a significant role as a navigation sensor for rendezvous and touchdown but also provides the length scale to generate a digital elevation map.

After the first use onboard the Apollo 15 mission to the Moon in 1971, laser altimeters have been widely used for many lunar, planetary and asteroid exploration missions requiring range measurements from tens of meter to hundreds of kilometers (Lim et al. 2016). These altimeters, based on the pulsed time-of-flight (TOF) technique, measure the round-trip time between the transmitted laser pulse and the echo pulse reflected from the target surface. The pulsed TOF altimeter requires high peak-power laser pulses (i.e., diode pumped Q-switched Nd:YAG lasers used for all space exploration missions), thereby causing not only high cost but also large requirements of size, weight and power (SWaP). A laser altimeter, based on the pseudo-random noise (PRN) modulation technique (Takeuchi et al. 1983), transmits laser pulse trains modulated with a PRN binary sequence on continuous wave (CW) laser sources and then receives echo pulse trains. The range is calculated from the peak of cross correlation in the time domain between the original binary sequence and received pulse trains. But the ranging accuracy is limited by the sampling rate of the analog-to-digital converter, the bit width or chip time of the PRN code, and signal-to-noise ratio (SNR). The PRN modulation technique has been used to extensive of applications for range-resolved measurements (e.g., robotics, remote sensing and autonomous driving) because of its capability to recover weak signals buried in random noise, including background noise. It was also proposed for satellite laser ranging (Norman & Gardner 1988) and laser altimeters for asteroid or comet exploration (Sun et al. 2007; Sun et al. 2021). In addition, the PRN modulation technique was applied to detect gravitational waves via bidirectional laser link of three satellites separated by 5 million kilometers forming an equilateral triangle (Esteban et al. 2010).

Unlike pulsed TOF altimeters, PRN altimeters allow low power CW diode lasers which are commercially available and can increase an average power using a master oscillator fiber amplifier (MOFA). The CW diode lasers with the MOFA architecture has been demonstrated in most CubeSat optical communications owing to the compact and robust architecture and a high peak-to-average-power ratio (Lim et al. 2020). Thus, the PRN altimeter can be designed in a fast and cost-effective way with reducing SWaP requirements. However, the PRN altimeter has lower SNR than the pulsed TOF altimeter for the same average transmitted power, which limits the operational range and ranging accuracy. A laser altimeter in the Apophis mission will be activated in a proximity operation mode in which the line-of-sight velocity between a spacecraft and the asteroid varies from the order of centimeters to meters per second. A slow-moving spacecraft allows the accumulation of the received pulse trains during integration time to improve SNR of cross correlation, resulting in an extended operational range and high ranging accuracy.

In this study, we investigated two performance metrics of laser altimeter (i.e., detection probability and ranging accuracy) based on the PRN modulation technique for the proximity operation mode of the Apophis mission. For commercially available components and compatibility with SWaP requirements, the laser altimeter employs a CW laser diode based on the MOFA architecture and an avalanche photodiode (APD) in the analog mode operation. We derived not only the closed-form expression of detection probability in terms of Hermite polynomial, but also the new ranging accuracy model based on Gaussian error propagation by taking into account the sampling rate. The numerical simulation showed that the laser altimeter could achieve the ranging performance required for rendezvous mission by accumulating the received pulse trains.

2. PRINCIPLE OF PSEUDO-RANDOM NOISE MODULATION CW LASER ALTIMETER

2.1 Receiver Output Statistics

The PRN binary sequence has been widely used in spread spectrum communications as well as microwave ranging applications such as the global positioning system, which can be generated by a linear feedback shift register circuit and shows truly random statistical properties. In the case of PRN modulation CW laser altimeter, the transmitting laser is modulated with PRN codes resulting in a binary sequence and the received signals are then decoded to achieve range-resolved measurements.

Generally, the received signal $y(t)$ at the input to an APD detector can be expressed as a convolution of the transmitting signal $x(t)$ and the surface response function

$h(t)$ as follows:

$$y(t)=\int_{-\infty}^{\infty}x(t-t')h(t')dt'+b(t) \tag{1}$$

where $b(t)$ denotes background noise. The modulation of the transmitting signal with CW laser output power P_T is given by Eq. (2) (Takeuchi et al. 1983), and the surface response function is derived to Eq. (3) using the link equation (Lim et al. 2019) and the Dirac delta function $\delta(t)$:

$$x(t)=P_T\sum_{n=0}^{N-1}a_n\mathrm{Rect}(t-nT_c) \tag{2}$$

$$h(t)=\frac{\rho}{\pi}\frac{A_R}{R^2}\eta_T\eta_R\cdot\delta(t-\tau_{TOF}) \tag{3}$$

where a_n is the PRN binary sequence code of one or zero, Rect(t) is the unit-amplitude rectangular function pulse (i.e., Rect(t) = 1 for $0 \le t \le \tau_c$, elsewhere Rect(t) = 0), T_c is the chip width or bit width (known as the clock-period of the modulation), N is the number of chips in one PRN binary sequence period, ρ is the surface albedo, R is the range to the surface, A_R is the receiving area, τ_{TOF} is the TOF of laser pulses, and η_T and η_R are the efficiencies of the transmitting and receiving optical systems, respectively.

Using Eqs. (1-3), the received signal $z(t)$ at the APD output in terms of photoelectrons is given by

$$\begin{aligned}z(t)=&P_R\left(G\frac{\eta_D\lambda}{\hbar c}\right)\sum_{n=0}^{N-1}a_n\mathrm{Rect}(t-nT_c-\tau_{TOF})\\&+\left(G\frac{\eta_D\lambda}{\hbar c}\right)b(t)+w(t)\end{aligned} \tag{4}$$

in which

$$P_R=P_T\frac{\rho}{\pi}\frac{A_R}{R^2}\eta_T\eta_R \tag{5}$$

where P_R is the received signal power, η_D and G are the quantum efficiency and the gain of an APD detector, respectively, λ is the wavelength of the transmitting laser, $\hbar$ is the Plank's constant, c is the light speed, $w(t)$ is the additive noise including shot noise due to signal and background light, dark current and thermal noise.

It has been shown that the APD output in the analog mode operation is well approximated by Gaussian statistics of electrical charge characterized by the mean and variance (Abshire 1984; Sun et al. 1992). Considering the assumption that the background noise power is constant over the code time interval, the received average signal z_n for the n^{th} transmitting code, as the average number of photoelectrons accumulated over the chip width, is expressed as

$$\begin{aligned}\langle z_n\rangle&=\int_{n\tau_c+\tau_{TOF}}^{(n+1)\tau_c+\tau_{TOF}}\langle z(t)\rangle dt\\&=G\frac{\eta_D\lambda}{\hbar c}(P_Ra_n+P_{bg})T_c+\frac{GI_b}{q}T_c+\frac{I_s}{q}T_c\end{aligned} \tag{6}$$

in which

$$P_{bg}=L_\lambda\Omega_{FoV}\eta_RA_R\Delta\lambda_{filter} \tag{7}$$

where I_s and I_b are the APD surface and bulk leakage current, respectively, q is the electron charge, L_λ is the solar spectral radiance, Ω_{FoV} is the receiver field of view in steradians, and $\Delta\lambda_{filter}$ is the bandwidth of the optical bandpass filter. The variance of z_n is given by

$$\begin{aligned}\mathrm{var}(z_n)=&FG^2\frac{\eta_D\lambda}{\hbar c}(P_Ra_n+P_{bg})T_c\\&+FG^2\frac{I_b}{q}T_c+\frac{I_s}{q}T_c+\frac{2\kappa T_e}{q^2R_L}T_c\end{aligned} \tag{8}$$

where F is the excess noise factor, κ is the Boltzmann's constant, T_e is the temperature in Kelvin, and R_L is the load resistance of detector circuit.

2.2 Cross Correlation and Signal-to-Noise Ratio

An advantageous property of PRN binary sequence in range-resolved measurements is that it has no apparent correlation with not only other binary sequences but also itself unless it is perfectly aligned in the time domain (Sun et al. 2021). Using the bipolar PRN code with the definition of $a'_n=2a_n-1=(-1)^{a_n+1}$, the cross correlation between the original and bipolar PRN codes, known as the correlation property, is given by (Takeuchi et al. 1983)

$$C_0(k)=\sum_{i=0}^{N-1}a'_ia_{i+k}=\begin{cases}(N+1)/2 & for\ k=0(\mathrm{mod}\,N)\\0 & for\ k\neq0(\mathrm{mod}\,N)\end{cases} \tag{9}$$

The PRN binary sequence consists of one and zero codes (or on and off codes) occurring statistically at random, in which the number of one codes always exceeds the number of zero codes by one unit (i.e., $(N+1)/2$ one codes and $(N-1)/2$ zero codes). Therefore, the sum of bipolar PRN codes in one sequence is 1, known as the balance property (i.e., $\sum_{i=0}^{N-1}a'_i=1$).

Taking into consideration two properties of correlation and balance, the mean of cross correlation between the received pulse train and bipolar PRN binary sequence is

expressed as

$$\langle C_k \rangle = \sum_{n=0}^{N-1} \langle z_n \rangle a'_{n-k} = \begin{cases} \mu_{sp} = P_R G \frac{\eta_D \lambda}{\hbar c} \frac{N+1}{2} T_c + \left(P_{bg} G \frac{\eta_D \lambda}{\hbar c} + \frac{GI_b}{q} + \frac{I_s}{q} \right) T_c & for\ k = 0 (\mathrm{mod}\, N) \\ \mu_{sn} = \left(P_{bg} G \frac{\eta_D \lambda}{\hbar c} + \frac{GI_b}{q} + \frac{I_s}{q} \right) T_c & for\ k \neq 0 (\mathrm{mod}\, N) \end{cases} \tag{10}$$

where μ_{sp} and μ_{sn} are the mean values of peak and non-peak cross correlation, respectively. It is worth noting that the peak cross correlation is $(N + 1)/2$ times the number of received photoelectrons over a single pulse owing to the $(N + 1)/2$ transmitting pulses in one sequence, when neglecting the background noise and dark current. This feature allows the PRN modulation CW laser altimeter to use a low peak power laser such as a diode laser. With some mathematical effort, the variance of cross correlation is derived as

$$\begin{aligned} \mathrm{var}\left(C_k\right) = \sum_{n=0}^{N-1} \mathrm{var}\left(z_n a'_{n-k}\right) &= P_R F G^2 \frac{\eta_D \lambda}{\hbar c} \frac{N+1}{2} T_c \\ &+ N T_c \left(P_{bg} F G^2 \frac{\eta_D \lambda}{\hbar c} + F G^2 \frac{I_b}{q} + \frac{I_s}{q} + \frac{2\kappa T_e}{q^2 R_L} \right) \end{aligned} \tag{11}$$

Eq. (11) shows that the variance has the same value for the peak and non-peak cross correlations (i.e., $\sigma_{sp}^2 = \sigma_{sn}^2 = \mathrm{var}\left(C_k\right)$), where σ_{sp}^2 and σ_{sn}^2 are the variances of the peak and non-peak cross correlations, respectively.

To achieve a sufficiently high value of the peak cross correlation for reliable detection, it is necessary to accumulate the received pulse trains whenever the transmitting signal sequence is repeated, and then cross correlate the accumulated trains with the original PRN binary sequence. By applying the accumulated trains over M times sequence to Eqs. (10) and (11), the mean and variance of cross correlation are achievable by multiplying Eqs. (10) and (11) by M of the accumulation number:

$$\langle C_k \rangle = \sum_{n=0}^{M(N-1)} \langle z_n \rangle a'_{n-k} = \begin{cases} \mu_p = M \mu_{sp} \\ \mu_n = M \mu_{sn} \end{cases} \tag{12}$$

$$\mathrm{var}\left(C_k\right) = \sum_{n=0}^{M(N-1)} \mathrm{var}\left(z_n a'_{n-k}\right) = \sigma_p^2 = \sigma_n^2 = M \sigma_{sp}^2 \tag{13}$$

In the case of PRN modulation CW laser altimeter, SNR is defined as the ratio of the mean value to the standard deviation for the peak cross correlation:

$$SNR = \frac{\langle C_k \rangle_{peak}}{\sqrt{\mathrm{var}\left(C_k\right)}} = \frac{\mu_p}{\sqrt{\sigma_p^2}} = \sqrt{M} \frac{\mu_{sp}}{\sqrt{\sigma_{sp}^2}} \tag{14}$$

The SNR is a significant figure to determine the ranging performance in terms of detection probability and ranging accuracy. It is noteworthy from Eq. (14) that SNR of M accumulated pulse trains is improved by $\sqrt{M}$ times, when compared to a received pulse train. However, the accumulation number of received pulse trains will not only affect the detection speed but also be limited by high-dynamic targets because the accumulated pulse trains are shifted in time corresponding to the line-of-sight velocity of target. The HgCdTe APD detector is a good candidate to increase SNR, which operates in a linear mode photon counting mode, and provides a quantum limited sensitivity. However, it requires a cryo-cooler resulting in large SWaP requirements (Sun et al. 2021).

3. PERFORMANCE METRICS

3.1 Detection Probability

The peak location of cross correlation gives the round-trip propagation time to the target because the received pulse train is correlated with delayed versions of the PRN binary sequence. Therefore, the target detection is achievable from a peak search of correlation functions that can be approximated as Gaussian random variables according to the central limit theorem. The detection probability is written as an open-form expression (Sun et al. 2021):

$$P_D = \left[\frac{1}{2\pi \sigma_p \sigma_n} \int_{-\infty}^{\infty} \exp\left(-\frac{\left(z_p - \mu_p\right)^2}{2\sigma_p^2} \right) \int_{-\infty}^{z_p} \exp\left(-\frac{\left(z_n - \mu_n\right)^2}{2\sigma_n^2} \right) dz_n dz_p \right]^{N-1} \tag{15}$$

Applying a Q-function and a Gauss-Hermite quadrature integration (Simon & Alouini 2000), Eq. (15) can be derived as the following closed-form and simple expression:

$$\begin{aligned} P_D &= \left[\frac{1}{\sigma_p \sqrt{2\pi}} \int_{-\infty}^{\infty} \exp\left(-\frac{\left(z_p - \mu_p\right)^2}{2\sigma_p^2} \right) Q\left(-\frac{z_p - \mu_n}{\sigma_n} \right) dz_p \right]^{N-1} \\ &= \left[\frac{1}{\sqrt{\pi}} \sum_{i=1}^{n} w_i Q\left(-\frac{\sqrt{2}\sigma_p x_i + \mu_p - \mu_n}{\sigma_n} \right) \right]^{N-1} \end{aligned} \tag{16}$$

where $Q(\cdot)$ is the Q-function, w_i and x_i denote the weight factors and the zero points of the n^{th}-order Hermite polynomial, respectively, whose values are well tabulated

(Ghassemlooy et al. 2018). The order of Hermite polynomial should be selected depending on the desired accuracy, which was taken as 20 in the numerical simulation.

3.2 Ranging Accuracy

The ranging accuracy in the PRN laser altimeter depends on four parameters: SNR, chip time, sampling time (i.e., sampling rate) and frequency stability of the on-board clock, which was investigated only by considering SNR and chip time (Buttgen et al. 2007; Ai et al. 2011; Sun et al. 2021). In this section, the ranging accuracy model is derived in terms of SNR, chip time and sampling time, based on the geometry of digital cross correlation function (CCF) as shown in Fig. 1.

The peak location of CCF is estimated using the two largest values of digital CCF (i.e., C_m and C_{m+1} in Fig. 1) which are located nearest to the peak location of CCF. In mathematical form, the ideal CCF can be expressed as (Buttgen et al. 2007)

$$C(t)=\begin{cases} C\max\left(1-\dfrac{|t-kNT_c|}{T_c}\right) & \text{for } \varepsilon_- < t < \varepsilon_+ \\ 0 & \text{elesewhere} \end{cases} \quad (17)$$

which represents a triangle with the width of $2T_c$ and boundary parameters of $\varepsilon_- = T_c(kN - 1)$ and $\varepsilon_+ = T_c(kN + 1)$, and $k \in Z$ means the periodic CCF. Based on the center of mass method using the two largest values, the round-trip time delay τ_{TOF} is calculated as

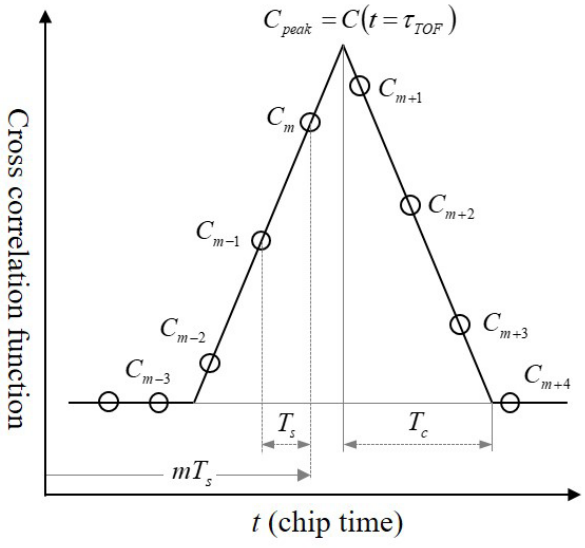

Fig. 1. Illustration of a digital CCF. T_s is the sampling time and m is the sample number corresponding to C_m before the digital CCF is maximal. CCF, cross correlation function.

$$\tau_{TOF}=\frac{C_m mT_s + C_{m+1}(m+1)T_s}{C_m + C_{m+1}} = mT_s + \frac{C_{m+1}T_s}{C_m + C_{m+1}} \quad (18)$$

By applying Gaussian error propagation, the standard deviation of Eq. (18) is expressed as

$$\sigma_{\tau_{TOF}} = \sqrt{\left(\partial\tau_{TOF}/\partial C_m\right)^2 \partial^2_{C_m} + \left(\partial\tau_{TOF}/\partial C_{m+1}\right)^2 \sigma^2_{C_{m+1}}} \quad (19)$$

where σ_{C_m} and $\sigma_{C_{m+1}}$ are the standard deviations of C_m and C_{m+1}, respectively. The partial derivatives are calculated as

$$\frac{\partial\tau_{TOF}}{\partial C_m} = \frac{-C_{m+1}}{\left(C_m + C_{m+1}\right)^2}T_s\,,\ \frac{\partial\tau_{TOF}}{\partial C_{m+1}} = \frac{C_m}{\left(C_m + C_{m+1}\right)^2}T_s \quad (20)$$

Let $\Delta\tau$ represent the time interval between C_m and C_{peak}. The sum of two digital CCFs in the denominator of Eq. (20) is obtained from Eq (17):

$$\begin{aligned} C_m + C_{m+1} &= C_{peak}\left(1-\frac{\Delta\tau}{T_c}\right) + C_{peak}\left(1-\frac{T_s-\Delta\tau}{T_c}\right) \\ &= C_{peak}\left(2-\frac{1}{\gamma}\right) \end{aligned} \quad (21)$$

where γ is the oversampling factor defined as the ratio of the chip time to the sampling time (i.e., T_c/T_s). In addition, we have the equation of $\sigma_{C_m} = \sigma_{C_{m+1}} = \sigma_{C_{\max}}$ which is reasonable from Eq. (11). The substitution of Eqs. (20) and (21) into (19) can be approximated as

$$\begin{aligned} \sigma_{\tau_{TOF}} &\approx \left(\frac{\gamma}{2\gamma-1}\right)^2 \frac{\sigma_{C_{peak}}}{C^2_{peak}}\left(\frac{T_c}{\gamma}\right)\sqrt{C^2_m + C^2_{m+1}} \\ &\le \left(\frac{\gamma}{2\gamma-1}\right)^2 \frac{\sigma_{C_{peak}}}{C^2_{peak}}\left(\frac{T_c}{\gamma}\right)\left(C_m + C_{m+1}\right) \\ &\approx \frac{1}{2\gamma-1}\frac{\sigma_{C_{peak}}}{C_{peak}}T_c \approx \frac{1}{2\gamma-1}\frac{T_c}{SNR_{peak}} \end{aligned} \quad (22)$$

Eq. (22) represents the standard deviation of the round-trip time delay. Thus the ranging accuracy or ranging standard deviation can be expressed as

$$\sigma_R \approx \frac{1}{2(2\gamma-1)}\frac{cT_c}{SNR_{peak}} \quad (23)$$

where the first term is related to the sampling time, which is not taken into account in the conventional expression

of ranging accuracy (i.e., $\gamma = 1$). It is worth noting that the ranging error is proportional to the chip time as well as the sampling time but inversely proportional to SNR corresponding to Eq. (14).

4. NUMERICAL RESULTS AND DISCUSSIONS

In this section, we address the numerical results to analyze the ranging performance, in terms of detection probability and ranging accuracy, of laser altimeter based on the PRN modulation technique for the proximity operation of the Apophis mission. The laser altimeter is required to have the ranging accuracy less than 100 cm tentatively in the proximity operation mode ranging from 50 m to 10 km.

The proximity operation will be conducted near the Earth, and thus the solar spectral irradiance is assumed to be $L_\lambda = 0.027$ W/cm^2 μm at one astronomical unit and 1,550 nm wavelength (Hemmati 2006). Apophis is classified as a Sq-type asteroid, and its albedo has been calculated as 0.33 ± 0.08 from polarimetric observations (Delbò et al. 2007), which is greater than 0.3 in the visible to near-infrared spectrum (Binzel et al. 2009). Consequently, we assume the albedo to be 0.33 in the simulation. The number of binary bits in the PRN code sequence is $N = 127$ which comes from seven stages in the shift register. The bit width is $T_c = 200$ ns and the oversampling factor is $\gamma = 20$ which results in the sampling time of $T_s = 10$ ns. Taking into account not only a CW laser diode based on the MOFA architecture but also an APD in the analog mode operation, the transmitter and receiver parameters are listed in Table 1.

Fig. 2 shows the original PRN binary sequence at 5 Mbps data rate (i.e., 200 ns bit width) which consists of 127 (2^7 – 1) bits generated by the seven linear feedback shift register. The sequence shows an almost uniform distribution of zeros and ones, including the balance and correlation properties.

Table 1. Transmitter and receiver parameters used in the numerical simulation

Parameter description	Symbol	Value
Laser wavelength	λ	1,550 nm
Average laser power	P_T	2 W
Tx optical efficiency	η_T	0.95
Effective Rx area	A_R	50.3 cm^2
Rx optical efficiency	η_R	0.74
Optical filter bandwidth	$\Delta\lambda_{filter}$	10 nm
Rx field-of-view	Ω_{FoV}	85 μrad
APD quantum efficiency	η_D	0.84
APD gain	G	40
APD excess noise factor	F	19.1
Surface dark current	I_s	20 nA
Bulk dark current	I_b	50 pA
Absolute temperature	T	293.5 K
Load resistance	R_L	2.75 kΩ

APD, avalanche photodiode.

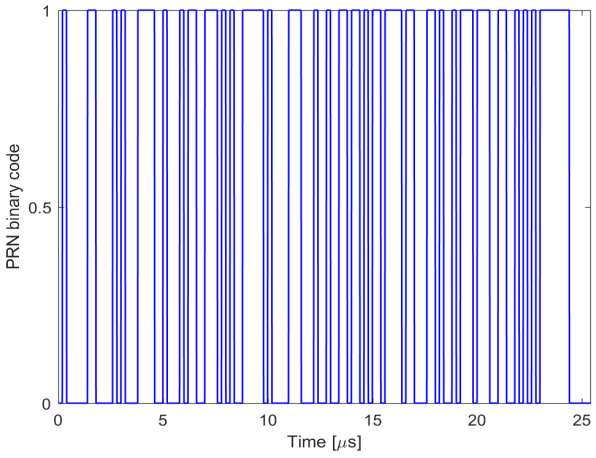

Fig. 2. Original pseudo-random noise binary sequence.

The number of received photoelectrons at the APD output over sampling time, which includes the additive noise, is shown in Fig. 3. The numerical simulation used a Gaussian random number generator based on Eqs. (6) and (8) to calculate the number of received photoelectrons. Compared to Fig. 3(a), the number of received photoelectrons in Fig. 3(b) is approximately 1,000 times greater due to the accumulation number. However, there is no distinct pattern similar to the PRN binary sequence, as shown in Fig. 2.

Figs. 4 and 5 show SNR for the peak cross correlation and detection probability, respectively, in terms of the operation range. The pulse broadening effect caused by the surface slope and roughness is negligible in calculating CCF, owing

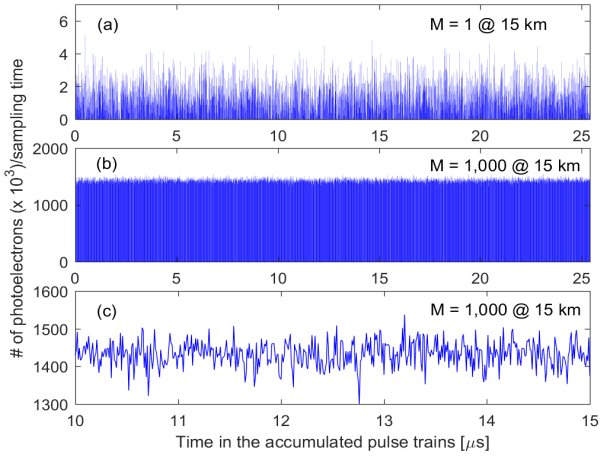

Fig. 3. The number of received photoelectrons per sampling time for two accumulated pulse trains ($M = 1$ and 1,000 at 15 km). Fig. 3(c) shows results corresponding to Fig. 3(b) over a finer time scale.

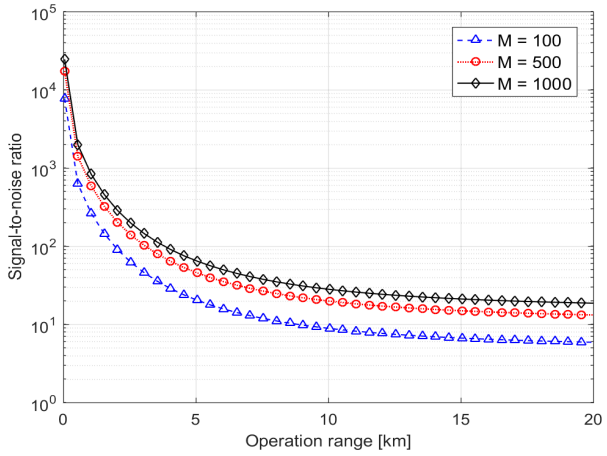

Fig. 4. Signal-to-noise ratio for the peak cross correlation in terms of the operation range.

to the small beam divergence angle and relatively wide bit width. As shown in Eq. (14), the accumulated pulse trains improve SNR by $\sqrt{M}$ times compared to a received pulse train with M = 1. Therefore, SNR for two accumulation numbers of M = 500 and 1,000 increases by $\sqrt{5}$ and $\sqrt{10}$ times, respectively, at the same operation range when compared to SNR employing M = 100. SNR for the peak cross correlation is considerably larger than 1 for three accumulation numbers, even at the operation range of 20 km. It means that the laser altimeter allows range-resolved measurements within the operation range of 20 km if the accumulation number is larger than 100. However, the range-resolved measurements are not reliable in the proximity operation with M = 1,000 and R = 20 km because the detection probability is approximately 22%, as shown in Fig. 5. It is concluded in terms of detection probability that

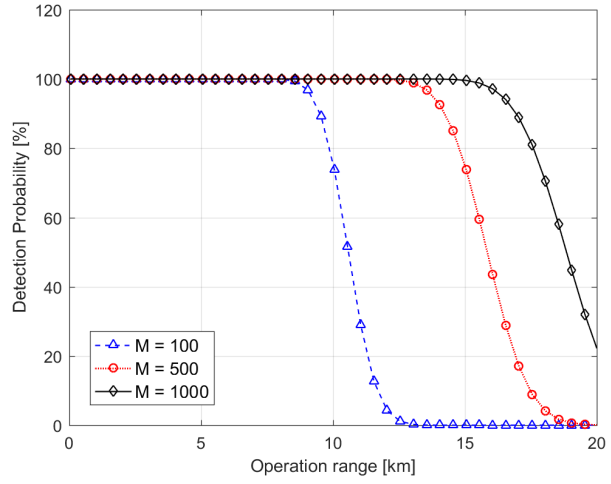

Fig. 5. Detection probability in terms of the operation range.

the maximum operation range of the laser altimeter is 15 km when employing M = 1,000, where detection probability is about 100%. SNR is, from the numerical simulation, dominated by thermal noise rather than shot noise and dark current. In the APD analog mode operation, using a larger load resistance reduces thermal noise, as shown in Eq. (8), thereby improving SNR. Consequently, the APD load resistance should be as large as possible to reduce the thermal noise current generated by the resistor. It is generally designed so that thermal noise reaches a level equal to shot noise while maintaining a high response speed.

For more intensive investigation of detection probability, the CCF, between the bipolar PRN binary sequence and the received pulse train, is shown in Fig. 6. As previously stated, the target detection is achievable from a peak search of CCF. Unlike Fig. 6(b), there is no apparent peak of CCF in Fig. 6(a) because the detection probability is approximately zero, as shown in Fig. 5, for the proximity operation with M = 100 and R = 15 km. However, we can find a peak of CCF in the range of 15 km, as shown in the circle of Fig. 6(b), owing to the detection probability of approximately 100%. The CCF value in Fig. 6(b) is 10 times greater than the CCF value at 15 km in Fig. 6(a), due to the larger accumulation number (i.e., M = 1,000), which can be inferred from Eq. (12). The cross correlation based on the PRN modulation technique provides an excellent tool for range-resolved measurements although the signal is buried in random noise, as shown in Fig. 3(b). Fig. 6(c) shows a triangle shape of peak CCF near 15 km, which is distorted from the ideal triangle by the additive noise. The distortion of a triangle is proportional to the strength of additive nose and makes it difficult to find an

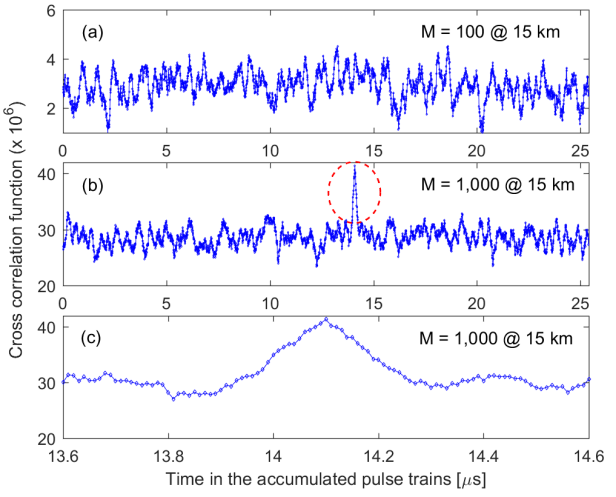

Fig. 6. Cross correlation functions for two accumulated pulse trains (M = 1 and 1,000 at 15 km). Fig. 6(c) shows results corresponding to Fig. 6(b) over a finer time scale.

accurate peak location of CCF, and consequently degrades the ranging accuracy.

Fig. 7 shows the ranging accuracy in terms of the operation range for three accumulated pulse trains. Given the sampling time and the bit width, the ranging error increases as the operation range is extended and the number of accumulated pulse trains becomes smaller, owing to SNR reduction. If the frequency stability of the on-board clock is neglected, the ranging accuracy is less than 15 cm for the operation range smaller than 20 km and an accumulation number larger than 100. In particular, the ranging accuracy is on the order of centimeters within the operation range of 15 km for 1,000 accumulated pulse trains. Taking into account the tentative requirements of proximity operation for the Apophis mission (i.e., ranging accuracy less than 100 cm in the operation range from 50 m to 10 km), the laser altimeter should be operated within the operation range of 15 km with 1,000 accumulated pulse trains, for reliable and robust range-resolved measurements in terms of the detection probability and the ranging accuracy.

5. CONCLUSION

A laser altimeter based on the PRN modulation technique was proposed for the proximity operation mode of the Apophis mission, and the performance metrics were evaluated in terms of the detection probability and the ranging accuracy. This technique allows a low peak power laser such as a diode laser, thereby enabling a compact and robust laser altimeter. The commercially available products were considered in the laser altimeter to meet SWaP requirements, which include not only a CW diode laser diode based on the MOFA architecture but also an APD detector in the analog mode operation. We derived two new mathematical models for the ranging performance evaluation: detection probability with a closed-form and ranging accuracy considering the sampling time. The accumulated pulse trains were employed to increase SNR of the peak cross correlation, which improves the SNR by $\sqrt{M}$ times compared to a received pulse train.

It was demonstrated that the laser altimeter was able to provide an excellent performance in the proximity operation mode (i.e., ranging accuracy on the order of centimeters and detection probability of 100%) within the operation range of 15 km for 1,000 accumulated pulse trains. The small accumulation number of received pulse trains should be applied to the high dynamic mode rather than the proximity operation mode, which leads to small SNR and then degrades the detection probability as well as the ranging accuracy. The laser altimeter is also available for the high dynamic mode by applying either a higher average power laser or an APD detector with a quantum limited sensitivity such as a HgCdTe detector. These components result in large SWaP constraints but should be also taken into consideration if the laser altimeter is required in the high dynamic mode of Apophis mission.

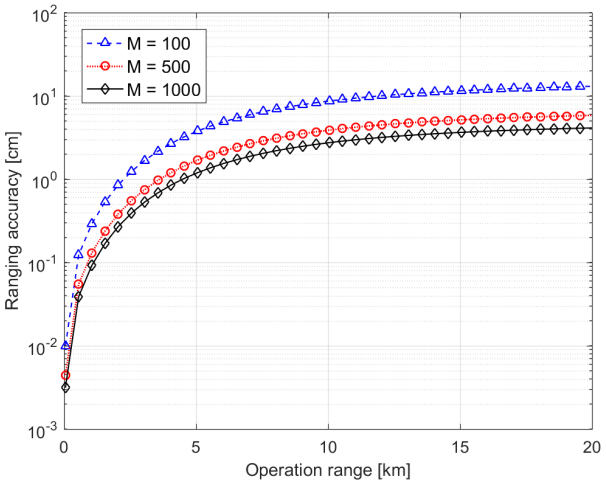

Fig. 7. Ranging accuracy in terms of the operation range.

ACKNOWLEDGMENTS

This work was supported by the Korea Astronomy and Space Science Institute through the project of "Physical and Dynamical Evolution of the Moon and Small Solar System Bodies" funded by the Ministry of Science and ICT (MSIT) of the Korean government.

ORCID

Hyung-Chul Lim https://orcid.org/0000-0001-5266-1335
Ki-Pyung Sung https://orcid.org/0000-0003-2639-4127
Mansoo Choi https://orcid.org/0000-0003-2019-3615
Jong Uk Park https://orcid.org/0000-0001-8060-6050
Chul-Sung Choi https://orcid.org/0000-0003-2004-2972
Seong-Cheol Bang https://orcid.org/0000-0002-2691-5976
Young-Jun Choi https://orcid.org/0000-0001-6060-5851
Hong-Kyu Moon https://orcid.org/0000-0001-5666-9967

REFERENCES

Abshire J, Performance of OOK and low-order PPM modulations in optical communications when using APD-based receivers, IEEE Trans. Commun. 32, 1140-1143 (1984). https://doi.org/10.1109/TCOM.1984.1095976

Ai X, Nock R, Rarity JG, Dahnoun N, High-resolution random-modulation cw lidar, Appl. Opt. 50, 4478-4488 (2011). https://doi.org/10.1364/AO.50.004478

Binzel RP, Rivkin AS, Thomas CA, Vernazza P, Burbine TH, et al., Spectral properties and composition of potentially hazardous asteroid (99942) Apophis, Icarus. 200, 480-485 (2009). https://doi.org/10.1016/j.icarus.2008.11.028

Brozović M, Benner LAM, McMichael JG, Giorgini JD, Pravec P, et al., Goldstone and Arecibo radar observations of (99942) Apophis in 2012–2013, Icarus. 300, 115-128 (2018). https://doi.org/10.1016/j.icarus.2017.08.032

Buttgen B, Mechat MAE, Lustenberger F, Seitz P, Pseudonoise optical modulation for real-time 3-D imaging with minimum interface, IEEE Trans. Circuits Syst. I Regul. Pap. 54, 2109-2119 (2007). https://doi.org/10.1109/TCSI.2007.904598

Delbò M, Cellino A, Tedesco EF, Albedo and size determination of potentially hazardous asteroids: (99942) Apophis, Icarus. 188, 266-269 (2007). https://doi.org/10.1016/j.icarus.2006.12.024

Esteban JJ, García AF, Eichholz J, Peinado AM, Bykov I, et al., Ranging and phase measurement for LISA, J. Phys. Conf. Ser. 228, 012045 (2010). https://doi.org/10.1088/1742-6596/228/1/012045

Ghassemlooy Z, Popoola W, Rajbhandari S, Optical Wireless Communications: System and Channel Modelling with MATLAB, 2nd ed. (CRC Press, Boca Raton, FL, 2018).

Hemmati H, Deep Space Optical Communications (John Wiley & Sons, Hoboken, NJ, 2006).

Lim HC, Kucharski D, Kim S, Choi CS, Sung KP, et al., Evaluation of a Geiger-mode imaging flash lidar in the approach phase for autonomous safe landing on the Moon, Adv. Space Res. 63, 1122-1132 (2019). https://doi.org/10.1016/j.asr.2018.10.028

Lim HC, Neumann GA, Choi MH, Yu SY, Bang SC, et al., Baseline design and performance analysis of laser altimeter for Korean lunar orbiter, J. Astron. Space Sci. 33, 211-219 (2016). https://doi.org/10.5140/JASS.2016.33.3.211

Lim HC, Yu SY, Sung KP, Park JU, Choi CS, et al., Performance analysis of M-ary optical communication over log-normal fading channels for CubeSat platforms, J. Astron. Space Sci. 37, 219-228 (2020). https://doi.org/10.5140/JASS.2020.37.4.219

Moon HK, Choi YJ, Kim MJ, Jeong Ahn Y, Yang H, et al., Apophis Rendezvous Mission for Scientific Investigation and Planetary Defense, in Apophis T-9 Years Workshop, Nice, France, 4-6 Nov 2020.

Norman DM, Gardner CS, Satellite laser ranging using pseudonoise code modulated laser diodes, Appl. Opt. 27, 3650-3655 (1988). https://doi.org/10.1364/AO.27.003650

Simon MK, Alouini MS, Digital Communication over Fading Channels: A Unified Approach to Performance Analysis (John Wiley & Sons, New York, NY, 2000).

Sun X, Abshire JB, Krainak MA, Hasselbrack WB, Photon counting pseudorandom noise code laser altimeters, Proceedings of SPIE 6771, Boston, MA, 9-11 Sep 2007.

Sun X, Cremons DR, Mazarico E, Yang G, Abshire JB, et al., Small all-range lidar for asteroid and comet core missions, Sensors. 21, 3081 (2021). https://doi.org/10.3390/s21093081

Sun X, Davidson FM, Boutsikaris L, Abshire JB, Receiver characteristics of laser altimeters with avalanche photodiodes, IEEE Trans. Aerosp. Electron. Syst. 28, 268-275 (1992). https://doi.org/10.1109/7.135452

Takeuchi N, Sugimoto N, Baba H, Sakurai K, Random modulation cw lidar, Appl. Opt. 22, 1382-1386 (1983). https://doi.org/10.1364/AO.22.001382

Thuillot W, Bancelin D, Ivantsov A, Desmars J, Assafin M, et al., The astrometric Gaia-FUN-SSO observation campaign of 99942 Apophis, Astron. Astrophys. 583, A59 (2015). https://doi.org/10.1051/0004-6361/201425603

Yu Y, Richardson DC, Michel P, Schwartz SR, Ballouz RL, Numerical predictions of surface effects during the 2029 close approach of asteroid 99942 Apophis, Icarus. 242, 82-96 (2014). https://doi.org/10.1016/j.icarus.2014.07.027